

# Two- and Three-Dimensional Photonic Crystals Built with VLSI Tools

Shawn-Yu Lin, J.G. Fleming, and E. Chow

## Introduction

The drive toward miniature photonic devices has been hindered by our inability to tightly control and manipulate light. Moreover, photonics technologies are typically not based on silicon and, until recently, only indirectly benefited from the rapid advances being made in silicon processing technology. In the first part of this article, the successful fabrication of three-dimensional (3D) photonic crystals using silicon processing will be discussed. This advance has been made possible through the use of integrated-circuit (IC) fabrication technologies (e.g., very large-scale integration, VLSI) and may enable the penetration of Si processing into photonics. In the second part, we describe the creation of 2D photonic-crystal slabs operating at the  $\lambda = 1.55 \mu\text{m}$  communications wavelength. This class of 2D photonic crystals is particularly promising for planar on-chip guiding, trapping, and switching of light.

## Design of 3D Photonic Crystals

Yablonovitch<sup>1</sup> and John<sup>2</sup> first proposed the modern photonic lattice concept in 1987. In general, the idea was to modulate photons in a manner similar to the way electrons are modulated in a semiconductor. This is achieved through a periodic variation in the refractive index. A pseudogap was first demonstrated theoretically in a macroscopic fcc structure with spherical airholes.<sup>3</sup> A design with a full bandgap based on diamond symmetry was proposed by Ho et al. of Iowa State University.<sup>4,5</sup> This design will be considered in the most detail here since it lends itself to microfabrication.<sup>6,7</sup> In the inset of Figure 1a, a scanning electron microscopy (SEM) image of such a 3D photonic crystal

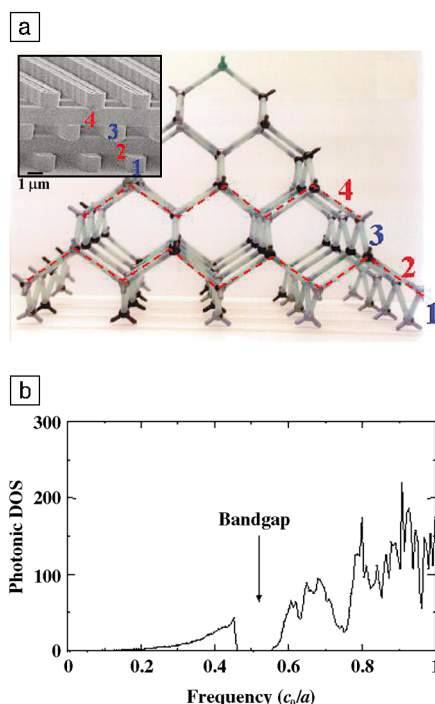


Figure 1. (a) A diamond lattice structure. The four layers of the unit cell are numbered. The inset shows a scanning electron microscopy (SEM) image of a three-dimensional (3D) silicon photonic crystal based on the layer-by-layer ("woodpile") structure. (b) A photonic density-of-states (DOS) spectrum calculated for the 3D crystal shown in the inset. The photonic DOS vanishes completely at  $\omega \sim 0.45\text{--}0.56$ , yielding a large photonic bandgap. The refractive index ( $n$ ) is 3.60; the material filling fraction is 0.28;  $c_0$  and  $a$  are the free-space speed of light and the lattice spacing, respectively.

tal, built up of stacked arrays of silicon bars, is shown. The corresponding diamond lattice structure and a calculated photonic density-of-states (DOS) spectrum are shown in Figures 1a and 1b, respectively. In short, the 1D rods each represent the shortest  $\langle 110 \rangle$  chain of atoms in a diamond lattice and are stacked like a woodpile. The stacking sequence is such that every four layers constitute a unit cell. For this structure, there is a frequency ( $f$ ) range in which the photonic DOS vanishes (a photonic bandgap), centered at  $f = 0.5 c_0/a$  (see Figure 1b), where  $c_0$  and  $a$  are the free-space speed of light and the lattice spacing, respectively.

Similar structures consisting of stacked rods have been generically described as "woodpile" structures.<sup>8</sup> A different design, which uses alternating rectangular rods and more closely mimics the arrangement of atoms in the diamond structure but which is more difficult to fabricate, has also been proposed.<sup>9</sup> Another structure with a full bandgap has been proposed by workers at the Massachusetts Institute of Technology (MIT).<sup>10</sup> The simple cubic structure is also predicted to have a full gap.<sup>11,12</sup> An interesting "triple-hole" structure has also been demonstrated.<sup>13</sup> We at Sandia National Laboratories have also proposed several structures, such as an inverse (reversed index contrast) "stick-figure" fcc structure,<sup>14</sup> as well as inverse "stick-figure" hcp and other high-symmetry structures.

During the evolution of these structures, a number of rules of thumb have been developed. Successful lattice designs often have a large contrast in refractive index, a high degree of symmetry, a spherical-like Brillouin zone, and interconnected regions of high-index material.

## Fabrication of 3D Photonic Crystals

Over the past decade, several of the designs proposed here have been fabricated. Since the dimensions of the lattice scale with the wavelength of light, it is a challenging task to fabricate infrared 3D photonic crystals ( $\lambda = 1\text{--}10 \mu\text{m}$ ) as the minimum feature size approaches micrometer and submicrometer length scales.

The approach we have taken in our work<sup>6,7</sup> has been to employ the woodpile structure initially proposed by a group at Iowa State University<sup>5</sup> and fabricate it using modified silicon IC fabrication processes. Two different processes were developed in the course of this work. The first process combined a series of mold definition, mold filling, and chemical-mechanical polishing (CMP) steps to create parts with a minimum feature size of  $1.2 \mu\text{m}$ .<sup>6</sup> The

second process allowed us to fabricate parts with minimum feature sizes of  $0.18 \mu\text{m}$ .<sup>7</sup> In "fillet" processing, the minimum feature size is determined by sidewall coverage of a deposited thin film. In all of the processes investigated, the use of CMP to maintain planarity is critical. CMP ensures that topography introduced in one layer does not propagate into subsequent levels. In this manner, the number of levels is limited only by the generation of stress on the wafer. At the end of the process, the silicon dioxide can be selectively removed using a hydrofluoric acid solution. The index contrast in our case is between polysilicon and the surrounding air and is therefore  $\sim 3.6:1$ . The filling fraction of the high-dielectric material is about 28%.

As examples of the flexibility of this approach, we have used it to fabricate not just the Iowa State<sup>4,5</sup> structure, but also the MIT structure<sup>10</sup> (Figure 2a), a  $90^\circ$  Iowa State (Ames) structure (Figure 2b), the simple cubic (SC) structure<sup>12</sup> (Figure 2c), an inverse fcc structure<sup>14,15</sup> (Figure 2d), an inverse

hcp structure, and the wurtzite structure. By fabricating the Iowa State structure at  $90^\circ$ , experimental determination of the gap at  $90^\circ$  becomes relatively easy. This particular structure is of sufficient complexity that it would be difficult to fabricate and test on a macroscopic scale. The A-B-C stacking sequence of an fcc structure is also indicated by circles in Figure 2d.

### Experimental Demonstration of a 3D Photonic Bandgap

As our approach is based on silicon IC processing, single-domain 3D photonic crystals can be fabricated on wafers as large as 6–12 in., with excellent uniformity. An SEM image of a large 3D silicon photonic crystal is shown in Figure 3a. In Figure 3b, the transmission spectrum through a three- and four-layer 3D crystal with a minimum feature size of  $0.18 \mu\text{m}$  is shown. In the allowed band ( $\lambda > 2.4 \mu\text{m}$ ), a 100% transmittance was observed for both samples, indicating that our structure has little, if any, absorption and scat-

tering loss. In the bandgap region of  $\lambda \sim 1.5 \mu\text{m}$ , a strong transmittance dip is observed. The manner in which the photonic bandgap develops with the addition of layers is also clearly seen. The size of the gap is large,  $\Delta\lambda \sim 400 \text{ nm}$ , and its attenuation strength is strong,  $\sim 2.5 \text{ dB/layer}$ . This structure has also been shown to have a 3D bandgap in all directions and for both polarizations, that is, a complete bandgap.<sup>16</sup>

To date, we have found the performance of these devices to be relatively insensitive to most processing parameters. Level-to-level alignment can deviate by as much as 10%, as can layer width and height, without seriously compromising performance. However, care must be taken to ensure that neighboring levels make physical contact if the silicon dioxide is to be removed at the end of the process.

### 3D Photonic-Crystal Waveguides, Bends, and Microcavities

To create optical functionality, defects must be introduced to disturb the periodic

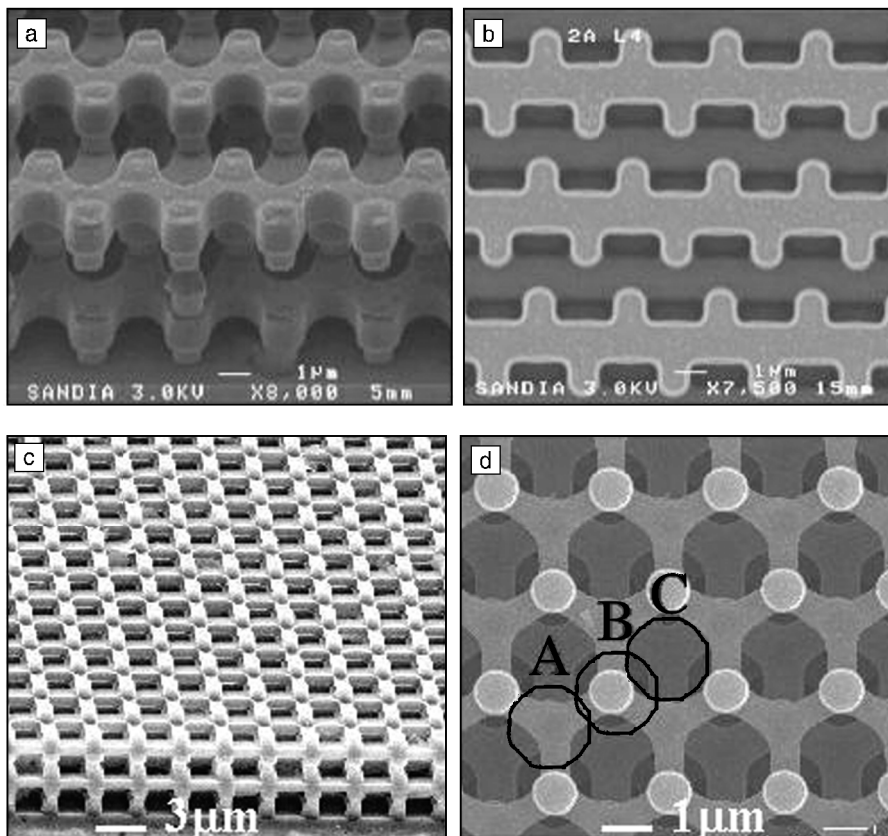


Figure 2. SEM images of a variety of 3D silicon photonic crystals, all fabricated using the same silicon integrated-circuit (IC) process technology. Structures with diamond symmetry, proposed by (a) MIT and (b) Iowa State University (Ames) are shown, as well as (c) simple cubic and (d) inverse fcc structures. The A-B-C stacking sequence of the fcc crystal symmetry is indicated by circles.

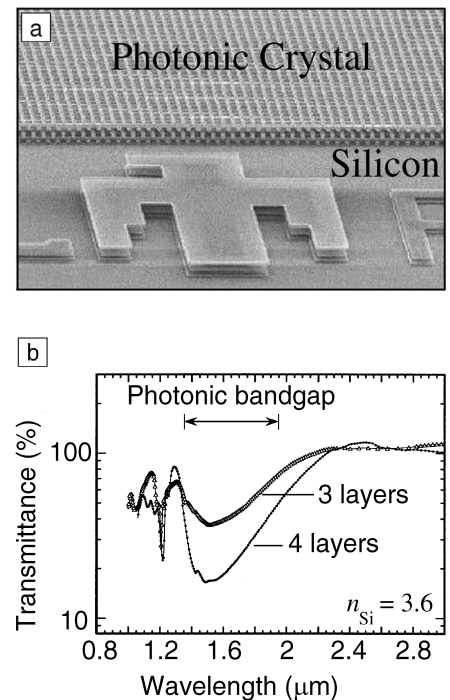


Figure 3. (a) SEM image of a large-area layer-by-layer 3D silicon photonic crystal. Its minimum feature size is  $0.18 \mu\text{m}$ , and the photonic bandgap occurs at  $\lambda \sim 1.5 \mu\text{m}$ . The photonic-crystal structure is uniform to better than 5% and is structurally coherent over the entire 6-in. wafer. (b) Transmission spectra of a 3D photonic crystal for three- and four-layer thicknesses ( $n$  is the refractive index).

dielectric structure. A linear waveguide is created by removing a single rod, thus forming a 1D optical channel. A waveguide bend can also be created by joining two linear waveguides at an intersection.<sup>17–19</sup> In this device, light propagates in air (the lower-index region), guided by the surrounding bandgap material. An SEM image of a linear waveguide fabricated in a 3D photonic crystal with a minimum feature size of  $0.8 \mu\text{m}$  is shown in Figure 4a. A simulation made using the finite-difference time-domain (FDTD) technique (see Figure 4b) shows that light can be steered around such a 3D waveguide bend without significant radiation loss.<sup>18</sup>

It is also possible to fabricate a photonic-crystal microcavity using our approach.<sup>20</sup> These cavities are the result of intentional structural point defects introduced into the lattice. The defects can either be additive (the addition of a line segment) or subtractive (the removal of a line segment). Figure 5 shows a transmittance spectrum taken from an additive-type cavity. The single peak at  $\lambda \sim 6.5 \mu\text{m}$  indicates the existence of a single-mode microcavity; the cavity quality factor ( $Q$ ) is  $\sim 300$ . The cavity modal volume is less than one cubic wavelength. This combination of a high- $Q$  and a small mode volume makes this microcavity very attractive for modifying spontaneous emission rate. This has potentially important implications for realizing single-mode light-emitting diodes and lasers.<sup>21,22</sup>

### Design of a 2D Waveguide-Coupled Photonic-Crystal Slab

A 2D photonic crystal is an attractive alternative and complement to its 3D counterpart, due to the simplicity of its fabrication. A 2D crystal confines light only in the 2D plane, however, and not in the third direction, the  $z$  direction. Earlier experiments showed that an ideal 2D system can exist.<sup>23–29</sup> Nonetheless, the usefulness of such 2D crystals is limited because they are less capable of guiding and controlling light in the  $z$  direction, which leads to diffraction loss. Here, we describe the successful nanofabrication of a waveguide-coupled 2D photonic-crystal slab.<sup>30,31</sup> The crystal slab has a strong 2D photonic bandgap at  $\lambda \sim 1.55 \mu\text{m}$ . More important, the crystal slab is capable of controlling light fully in all three dimensions, a prerequisite for realizing novel photonic-crystal devices such as thresholdless lasers.<sup>21,30,32</sup>

In the 2D plane, the basic crystal-slab structure consists of a simple 2D periodic dielectric array (see Figure 6a). In the  $z$  direction, it has a layered design with two important features. One is that the index

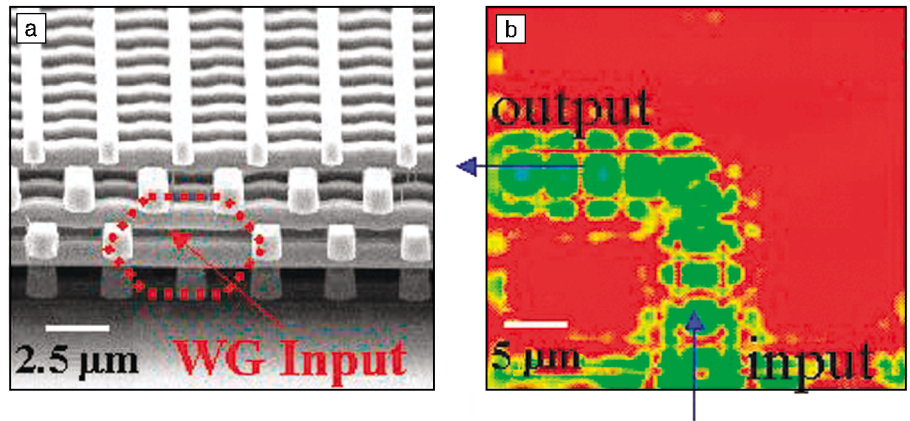


Figure 4. (a) SEM image of a 3D photonic-crystal waveguide based on the layer-by-layer structure in silicon; (b) a finite-difference time-domain (FDTD) simulation, showing the intensity profile of light (green color) propagating around a photonic-crystal waveguide bend with little bending loss.

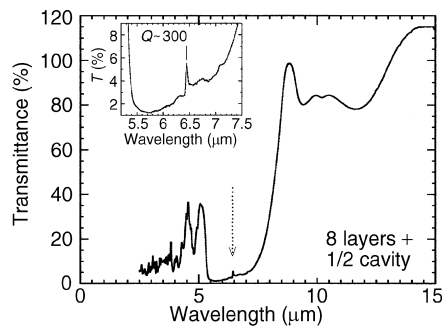


Figure 5. Measured transmission spectrum of a 3D photonic-crystal microcavity. The single peak at  $\lambda \sim 6.5 \mu\text{m}$  (shown by arrow) indicates the existence of a single-mode microcavity with a cavity quality factor  $Q$  of  $\sim 300$ . The inset graph shows the region around the  $6.5\text{-}\mu\text{m}$  peak in more detail.

contrast  $\Delta n$  between the waveguiding layer (GaAs,  $n \sim 3.5$ ) and the cladding layer ( $\text{Al}_x\text{O}_y$ ,  $n \sim 1.5$ ) is large ( $\Delta n \sim 2.0$ ).<sup>33,34</sup> Second, the high-index slab is thin, with a thickness  $t$  about half of the nearest hole-to-hole spacing  $a_0$ . Conventional waveguides, connected to a 2D hole array, are used for input and output coupling. The use of the underlying oxide has the added benefit of keeping the structure vertically attached, as opposed to a membrane structure, which is suspended in air.

The sample was grown by molecular-beam epitaxy on a GaAs substrate. Nanofabrication was accomplished using a combination of electron-beam lithography and reactive ion-beam etching (RIBE). After RIBE, the sample is placed in a hot

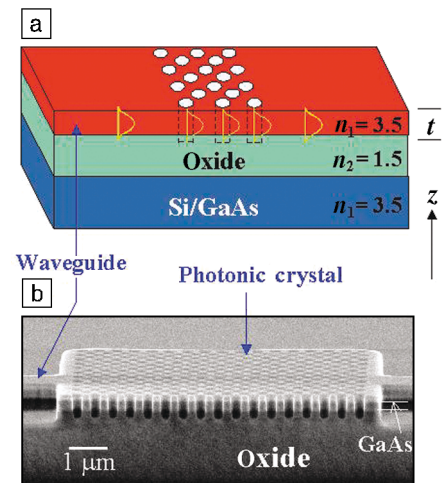


Figure 6. (a) Schematic drawing of a 2D photonic-crystal-slab design. There is a large index contrast,  $\Delta n \sim 2.0$ , between the guiding layer ( $n = 3.5$ ) and the oxide cladding layer ( $n = 1.5$ ). The thickness of the GaAs layer,  $t$ , is  $200 \text{ nm}$ . (b) SEM cross-sectional image of a fabricated 2D photonic-crystal slab. Conventional ridge waveguides, connected to a 2D hole array, are used for input and output coupling.

oven ( $420^\circ\text{C}$ ) for 20–30 min. This process converts the  $\text{Al}_{0.5}\text{Ga}_{0.1}\text{As}$  layer into an  $\text{Al}_x\text{O}_y$  layer, which acts as a cladding layer. An SEM cross-sectional image of the fabricated sample is shown in Figure 6b. For this particular sample, the GaAs thickness  $t = 200 \text{ nm}$ , the lattice constant  $a_0 = 400 \text{ nm}$ , and the hole diameter  $d = 240 \text{ nm}$ . The fabrication is nearly perfect, having a periodic 2D triangular array and straight etched holes.

### Demonstration of 2D Guided Modes and 2D Bandgaps

To find the absolute intrinsic transmittance of a 2D crystal, a reference transmission spectrum is taken from an identical waveguide with no 2D hole array built in the middle section. By rationing transmission signals, taken with and without a 2D crystal, intrinsic transmittance is obtained. This procedure eliminates external uncertainties associated with reflection at both the waveguide–crystal and the waveguide–air interfaces. Consequently, the normalization procedure allows for a better determination of intrinsic transmittance of a 2D crystal slab.

In Figure 7a, the measured and calculated TE (transverse electric) transmission spectra are plotted as black dots and a solid line, respectively. The frequency is expressed in a reduced unit  $\omega (a_0/\lambda)$  and is controlled by varying  $\lambda$  and  $a_0$  independently. Here,  $a_0 = 400$  nm, 430 nm, and 460 nm, and  $\lambda$  is tuned to 1320–1380 nm, 1520–1580 nm, and 1620–1685 nm, respectively. In the allowed band,  $\omega < 0.245$ , light is guided and propagates freely in the 2D plane. In the bandgap,  $\omega \sim 0.27$ , transmittance as low as  $\sim 2 \times 10^{-4}$  is observed. This is the condition at which light is guided vertically by strong index guiding and controlled horizontally by the 2D bandgap. It is in this sense that light can be controlled in all three dimensions using a 2D photonic-crystal-slab structure. The upper and lower TE band edges occur at  $\omega_1 \sim 0.34$  and  $\omega_2 \sim 0.25$ , respectively, yielding a large gap-to-midgap frequency ratio of 30%.<sup>30</sup>

### 2D Photonic-Crystal Waveguides and Waveguide Bends

A photonic-crystal waveguide can be created by introducing a triple line defect into a periodic 2D hole array (Figure 7b). The linear defect acts as a highly efficient 1D optical channel for light-guiding in the GaAs high-index layer. The defect hole diameter ( $d = 0.8a$ , where  $a$  is the lattice parameter) is slightly bigger than that of the regular holes ( $d = 0.6a$ ). It is noted that a single line defect also supports a guiding mode, but its center frequency is too close to the lower photonic-band edge. On the other hand, a triple line defect structure has an effective index lower than that of a single line defect, thus pushing the guided-mode frequency away from the lower band edge and more into the bandgap.<sup>31</sup>

In Figure 7a, the measured and calculated guiding efficiencies are shown as red triangles and a red line, respectively. An efficient guiding of light is observed at  $\omega = 0.26$ – $0.29$ , consistent with the theoretical prediction. Moreover, while

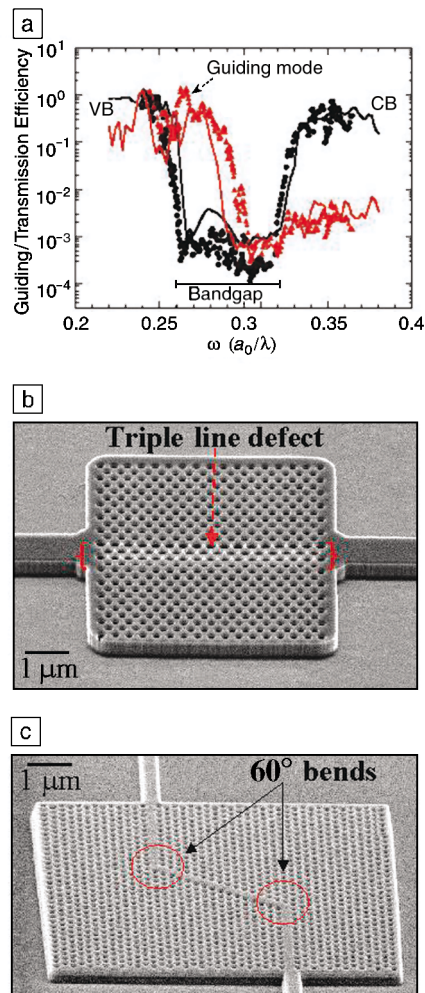


Figure 7. (a) Transmittance of a bulk 2D photonic-crystal slab (solid circles) and guiding efficiency of the triple line waveguide in (b) (red triangles). The calculated theoretical values are shown by the solid lines; measured values are shown by the respective symbols. VB indicates the valence band, CB indicates the conduction band. (b) SEM image of a photonic-crystal linear waveguide in GaAs. The waveguide consists of a triple line defect with a hole diameter ( $d = 0.8a$ ) larger than that of the regular holes ( $d = 0.6a$ ). (c) SEM image of  $60^\circ$  waveguide bend. Two  $60^\circ$  bends are used to form a double-bend device so that the input and output light are parallel to each other.

photonic-bandgap attenuation is strong ( $T \sim 4 \times 10^{-4}$ ) at  $\omega \sim 0.265$ , a near-perfect guiding efficiency of  $\sim 100\%$  is observed. This correlation confirms that guiding of light in this device is caused by the formation of a triple line defect and by the existence of a photonic bandgap.

The ability to bend light sharply and effectively is important for optical signal routing at  $1.55 \mu\text{m}$ . Based on the same slab structure, a  $60^\circ$  photonic-crystal bend can be successfully fabricated<sup>35</sup> (see Figure 7c). The bend has a compact bending radius of  $\sim 1 \mu\text{m}$  and is useful for connecting different optical components in a compact way. Two  $60^\circ$  bends are used to form a double-bend device so that the input and output light are parallel to each other. The ridge input and output waveguides are designed to have a lateral width of  $3^{1/2}a$  to better match the modal extent of the photonic-crystal waveguide. The measured bending efficiency shows a clear maximum value of  $\sim 100\%$  at  $\omega_{\text{max}} = 0.272$ , but with a narrow bandwidth,  $\Delta\lambda \sim 30$  nm. Future efforts must be concentrated on improving the bending bandwidth to  $\Delta\lambda \sim 100$  nm. The coupling efficiency between the ridge waveguide and the photonic-crystal waveguide must also be improved for practical applications.

### Summary

Basic 2D and 3D photonic-crystal structures operating at optical wavelengths have been experimentally realized in Si and GaAs. The next challenge in photonic-crystal research is to integrate superior photonic-crystal devices on-chip, compactly and effectively. The resulting optical subsystems will have an enhanced optical functionality to meet, for example, the needs for high-bandwidth communications networks. Another equally important challenge is in the integration of optically functional materials with a photonic crystal to achieve active photonic-crystal devices. Two distinct examples are the introduction of nonlinear materials for high-speed optical switching and the infiltration of a gain medium for highly efficient light-emitting applications.

### References

1. E. Yablonovitch, *Phys. Rev. Lett.* **58** (1987) p. 2059.
2. S. John, *Phys. Rev. Lett.* **58** (1987) p. 2486.
3. E. Yablonovitch and T.J. Gmitter, *Phys. Rev. Lett.* **63** (1989) p. 1950.
4. K.M. Ho, C.T. Chan, C.M. Soukoulis, R. Biswas, and M.M. Sigalas, *Solid State Commun.* **89** (1994) p. 413.
5. E. Ozbay, A. Abeyta, G. Turtle, M. Tringides, R. Biswas, C.M. Soukoulis, C.T. Chan, and K.M. Ho, *Phys. Rev. B* **50** (1994) p. 1945.
6. S.Y. Lin, J.G. Fleming, D.L. Hetherington, B.K. Smith, R. Biswas, K.M. Ho, M.M. Sigalas, W. Zubrzycki, S.R. Kurtz, and J. Bur, *Nature* **394** (1998) p. 251.
7. J.G. Fleming and S.Y. Lin, *Opt. Lett.* **24** (1999) p. 49.
8. H. Sozuer and J. Dowling, *J. Mod. Opt.* **41** (1994) p. 231.
9. K.M. Leung, *Phys. Rev. B* **56** (1997) p. 3517.

10. S.H. Fan, P.R. Villeneuve, R.D. Meade, and J.D. Joannopoulos, *Appl. Phys. Lett.* **65** (1994) p. 1466.
11. M. Wada, Y. Doi, K. Inoue, J.W. Haus, and Z. Yuan, *Appl. Phys. Lett.* **70** (1997) p. 2966.
12. S.Y. Lin, J.G. Fleming, R. Lin, M.M. Sigalas, R. Biswas, and K.M. Ho, *J. Opt. Soc. Am. B* **18** (2001) p. 32.
13. C.C. Cheng, V. Arbet-Engels, A. Scherer, and E. Yablonovitch, *Phys. Scr., T* **68** (1996) p. 17.
14. J.G. Fleming and S.Y. Lin, in *Proc. SPIE Photonics Technology into the 21st Century: Semiconductors, Microstructures, and Nanostructures*, Vol. 3899, edited by S.T. Ho, Y. Zhou, W.W. Chow, and Y. Arakawa (SPIE—The International Society for Optical Engineering, Bellingham, WA, 1999) p. 258.
15. S.G. Johnson and J.D. Joannopoulos, *Appl. Phys. Lett.* **77** (2000) p. 3490.
16. S.Y. Lin and J.G. Fleming, *IEEE J. Lightwave Technol.* **17** (1999) p. 1944.
17. S.-Y. Lin, E. Chow, V. Hietala, P.R. Villeneuve, and J.D. Joannopoulos, *Science* **282** (1998) p. 274.
18. M.M. Sigalas, R. Biswas, K.M. Ho, C.M. Soukoulis, D. Turner, B. Vasilii, S.C. Kothari, and S. Lin, *Microwave Opt. Tech. Lett.* **23** (1999) p. 56.
19. A. Chutinan and S. Noda, *Appl. Phys. Lett.* **75** (1999) p. 3739.
20. S.-Y. Lin, J.G. Fleming, M.M. Sigalas, R. Biswas, and K.M. Ho, *Phys. Rev. B* **59** (1999) p. 579.
21. E. Yablonovitch, *J. Opt. Soc. Am. B* **10** (1993) p. 283.
22. J.D. Joannopoulos, R.D. Meade, and J.N. Winn, *Photonic Crystals* (Princeton University Press, Princeton, NJ, 1995).
23. S.Y. Lin, G. Arjavalingam, and W.M. Robertson, *J. Mod. Opt.* **41** (1994) p. 385.
24. U. Gruning and V. Lehmann, *Thin Solid Films* **276** (1996) p. 151.
25. A. Rosenberg, R.J. Tonucci, H.B. Lin, and A.J. Campillo, *Opt. Lett.* **21** (1996) p. 830.
26. T.F. Krauss, R.M. De La Rue, and S. Brand, *Nature* **383** (1996) p. 699.
27. D. Labilloy, H. Benisty, C. Weisbuch, T.F. Krauss, R.M. De La Rue, V. Bardinal, R. Houdre, U. Oesterle, D. Cassagne, and C. Jouanin, *Phys. Rev. Lett.* **79** (1997) p. 4147.
28. H. Benisty, D. Labilloy, C. Weisbuch, M. Rattier, C.J.M. Smith, T.F. Krauss, R.M. De La Rue, R. Houdre, V. Bardinal, U. Oesterle, C. Jouanin, and D. Cassagne, *IEEE J. Lightwave Technol.* **17** (1999) p. 2063.
29. M. Kanskar, P. Paddon, V. Pacradouni, R. Morin, A. Busch, and J.F. Young, *Appl. Phys. Lett.* **70** (1997) p. 1438.
30. E. Chow, S.Y. Lin, S.G. Johnson, P.R. Villeneuve, J.D. Joannopoulos, J.R. Wendt, G.A. Vawter, W. Zubrzycki, H. Hou, and A. Alleman, *Nature* **407** (2000) p. 983.
31. S.Y. Lin, E. Chow, S. Johnson, and J.D. Joannopoulos, *Opt. Lett.* **25** (2000) p. 1297.
32. O. Painter, R.K. Lee, A. Scherer, A. Yariv, J.D. O'Brien, P.D. Dapkus, and I. Kim, *Science* **284** (1999) p. 1819.
33. P.R. Villeneuve, S. Fan, S.G. Johnson, and J.D. Joannopoulos, in *IEE Proc. Optoelec.*, Vol. 145 (Institution of Electrical Engineers, London, 1998) p. 384.
34. S.G. Johnson, S. Fan, P.R. Villeneuve, and J.D. Joannopoulos, *Phys. Rev. B* **60** (1999) p. 5751.
35. E. Chow, S.Y. Lin, J.R. Wendt, S.G. Johnson, and J.D. Joannopoulos, *Opt. Lett.* **26** (2001) p. 286. □

### Applications of Neutron Scattering to Materials Science and Engineering Oak Ridge, TN, October 1-3, 2001

#### Joint Institute for Neutron Sciences

##### Tutorial on Engineering Applications of Neutron Diffraction

October 1-2, 2001

*This tutorial will*

- Introduce neutron scattering to academic and industrial communities
- Provide an environment for learning the basics of stress mapping, texture measurement, and characterization of microstructure
- Promote the growth of a user community

##### Symposium on Fundamental Studies of Materials Phenomena Using Neutrons

October 2-3, 2001

*This symposium will*

- Introduce the capabilities of next-generation neutron scattering instruments
- Identify new and exciting research opportunities that will have a high impact on metals, ceramics, and engineering sciences

Registration fee: \$250 with scholarships available.

Additional details and registration information is available at [www.sns.gov/snsnews/jins.html](http://www.sns.gov/snsnews/jins.html)

**Location:** Spallation Neutron Source Building, 701 Scarboro Road, Oak Ridge, TN

**Contacts:** Technical information: Xun-li Wang (865) 574-9164 • [wangxl@sns.gov](mailto:wangxl@sns.gov)  
Local contact: Al Ekkebus (865) 241-5644 • [ekkebusae@sns.gov](mailto:ekkebusae@sns.gov)

**Sponsors:** Oak Ridge Associated Universities, Oak Ridge National Laboratory, University of Tennessee, Georgia Institute of Technology, North Carolina State University



Circle No. 10 on Inside Back Cover